Investigating the CoS_2 Mass Fraction Enhancing Performance Supercapacitor for Medium Low Consumption

Markus Diantoro[1,2*], *Nando* Dyas Arya[1], *Ishmah* Luthfiyah[1], *Herlin* Pujiarti[1], and *Santi* Maensiri[3]

[1]Department of Physics, Faculty of Mathematics and Natural Science, Universitas Negeri Malang, Jl. Semarang 5, Malang 65145, Indonesia
[2]Center of Advanced Materials for Renewable Energy, Universitas Negeri Malang, Jl. Semarang 5, Malang 65145, Indonesia
[3]School of Physics, Institute of Science, Suranaree University of Technology, Nakhon Ratchasima 3000, Thailand

Abstract. Supercapacitor are one of the most environmentally friendly electrical energy storage devices. Improvement of supercapacitor performance continues to be carried out by combining active materials and transition metal oxides/hydroxides. In this study, a composite electrode material based on activated carbon with a mass percent variation of CoS_2 has been successfully carried out. The composition of $Ni(OH)_2$-CoS_2/Graphene Nanosheet//Carbon electrode consists of 10, 15, and 20% CoS_2. The electrodes were then characterized using X-Ray Diffraction (XRD), Scanning Electron Microscope - Energy Dispersive X-ray (SEM-EDX). The research was continued by fabricating a symmetric coin cell. Supercapacitor device performance was characterized using Cyclic Voltammetry (CV), Charge-Discharge (CD) and Electrochemical Impedance Spectroscopy (EIS). The morphology of activated carbon shows porous chunks that are beneficial in the electrolyte ion adsorption process. While CoS_2 and Ni(OH)2 materials indicated in bulk form. Characterization results show the most optimum sample is in the 15% CoS_2 sample with EIS characterization showing the smallest equivalent series resistance (ESR) of 0.81 Ω. CD characterization results were able to have specific capacitance, energy density and power density of 58.25 Fg-1, 1.59 Wh/kg, and 70.49 W/kg respectively and were able to survive up to 88.84% after 1000 test.

1 Introduction

Energy demand is increasing rapidly globally in the coming years to be 10 times higher than current needs, as a result of which alternative energy development and modern product services are needed [1]. Along with the development of alternative energy, it is also necessary to store energy like batteries that have high energy density and supercapacitors that have high power density [2], [3]. Combining the two properties of energy storage devices such as

* Corresponding author: markus.diantoro.fmipa@um.ac.id.

batteries that have high specific energy and supercapacitors that have high specific power is the most logical way to get a better energy storage device, this tool is commonly called a supercapacitor [4]. Recently supercapacitor (supercapacitor + battery) has become a new proposal as an energy storage device that utilizes both capacitive and faradic charge storage mechanisms. Capacitive charging can be non-faradic (EDLC) or faradic (pseudocapacitive) or even both, while faradic charging can be either capacitive (pseudocapacitive) or non-capacitive (battery) [5]. So supercapatteries combine these to achieve high specific power capability like supercapacitors and high specific energy storage like batteries [6]. Theoretical capacitance of supercapacitor reaches 2575 Fg-1 and has advantages such as high conductivity, harmless to nature and good mechanical resistance [7].

Redox-active transition metal oxides and hydroxides, such as MnO^2 [8], Fe_2O_3 [9], CuO [10], $Co(OH)_2$ [11], NiO [12] and $Ni(OH)_2$ [13] are good materials as battery-type electrode materials due to their high theoretical specific capacitance with fast redox reactions on the surface. Nickel hydoxide Ni(OH)2 has recently been investigated as an electrode that has high power and energy density compared to carbon-based electrodes and better cyclic ability than polymer conductive materials[14]. Cobalt-based transition metals such as cobalt sulfide (CoS_2) are battery-grade electroactive materials [15]. Cobalt sulfide (CoS_2) with a wide variety of structures, catalyst activity, good conductivity, greater electrochemical properties and high theoretical capacitance (720 Fg-1) has been widely investigated in various energy devices [16]. CoS_2 is used as electrode material due to its good electrochemical activity, high thermal conductivity and low cost when compared to other cobalt metals[17]. In various research reports cobalt is used as an electrode material because it provides a more optimal oxidation potential besides that cobalt also has an atomic radius and ionization energy that can form favorable bimetallic compounds [18]. The synergy effect of bimetallic construction between cobalt and other metals is beneficial in optimizing the electronic structure, increasing the number of active sites and improving conductivity. Lightweight electrodes for commercial applications in the form of coin cells determine the specific capacitance which is usually calculated from the weight of the active material, besides the absence of polymeric materials commonly used in conventional methods in the fabrication process can improve the conductivity of the electrode [19], [20]. Previous studies have investigated nanostructured CoS_2 with a diversity of morphologies, such as nanosheets [21], nanotubes [22] and nanoneedles [23]. Research on $Ni(OH)_2$-CoS_2 composite materials needs to be carried out both from the micro/nano structure with a combination of other materials with high electroconductivity and good reactive properties.

Previous research successfully synthesized CoS/MXene/PANI producing a capacitance of 246 Fg^{-1} at a current density of 2 Ag^{-1}, another study successfully synthesized CoS2/PCNF with a capacitance of 688.8 Fg^{-1} at a current density of 1 Ag^{-1} and research on MnS_2@CoS_2 produced a capacitance value of 1158 Fg^{-1} at a current density of 1 Ag^{-1} [24 – 26]. Some studies report that metal (hydro)oxides present on graphene achieve better performance [27]. This electrode capacitance measurement is carried out using a 3-cell electrode system that is not yet in the form of a device so it is necessary to conduct research and fabrication in the form of a device such as a coin cell so that it can be applied directly to electronic devices.

2 Methods

The materials used in the synthesis were $Co(SO)_4$, N_2H_4, $Ni(NO_3)_2$ Graphene nanosheets, PVDF, DMAC, activated carbon, carbon black, Ethanol, Alcohol, DI water, cloth fiber and Et_4NBF_4. In the first stage, 9.8 grams of $Ni(NO_3)_2.6H_2O$ was dissolved in 60 mL of DI water with magnetic stirring at 50 ˚C for 1 hour. Next, 3 grams of NaOH was dissolved in 150 mL DI water with magnetic stirring at room temperature for 1 hour. The NaOH solution that has been made is dripped little by little on the Ni $NO_3)_2.6H_2O$ solution that has been

homogenized under magnetic stirring at 50 ˚C for 30 minutes. Then the sample was annealed at 150 ˚C for 11 hours. CoS2 powder was prepared by synthesizing $Co(SO)_4.{}_7H_2O$ (0.56 grams, 2 mmol) dissolved in 70 ml DI water to obtain a dark red solution. After that N2H4, $Ni(NO_3)_2$ (80%) was added dropwise using a pipette into the stirring solution until the final pH increased to 7.7. The resulting solution was kept stirring for 8 hours until a bluish precipitate. The precipitate was washed with DI water and ethanol and annealed at 60°C for 12 hours. Preparation of electrodes was carried out by dissolving 35 mg of PVDV binder in 2 ml DI Water through magnetic stirring for 30 minutes. $Ni(OH)_2$ and CoS_2 powders were then added with magnetic stirring at room temperature. Next, 10 mg of graphene was added with continued magnetic stirring for 24 hours until the solution was homogeneous. AC/CB composite paste was produced by mixing 80 mg of activated carbon, 100 mg of PVDF and 10 mg of Carbon Black into 5 mL of DMAC solution until a homogeneous solution was obtained. GNSs/$Ni(OH)_2$-CoS_2 composite solution and AC/CB composite were deposited on aluminium foil substrate. Then, each was dried in an oven at 100 ˚C for 1 hour. The fabrication of the supercapacitor coin cell consists of three components: electrode, electrolyte and separator (Figure 1). Electrodes of GNSs/$Ni(OH)_2$-$Co(OH)_2$ film and activated carbon film with a circular shape of 1 cm diameter were prepared as much as 1 sheet. The electrolyte used is Et_4NBF_4 and the separator is cloth fiber with the same size.

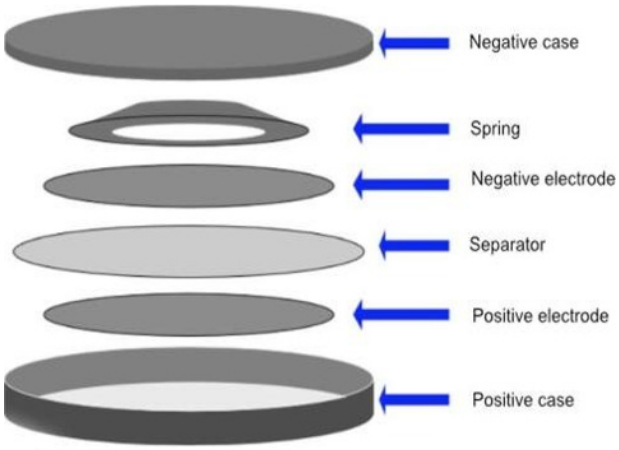

Fig. 1. Schematic of coin cell fabrication

3 Result and Discussion

XRD diffraction pattern of CoS_2 powder where the phase formed is amorphous. The results of the diffraction peak matching analysis indicate that the powder formed is CoS_2. Based on the analysis, the X-ray diffraction pattern shows that CoS_2 powder has peaks at diffraction angles $2\theta = 8.56º$, 23.73º and 27.34º in accordance with the JCPDS 70- 2866. The electrodes of each variation were also characterized by XRD to determine the composite material. The analysis showed the presence of $Ni(OH)_2$ peaks at diffraction angles $2\theta = 19.19°$, 33.27°, and 38.80°. While the CoS_2 peak is not visible due to its amorphous structure similar to the structure of activated carbon. Activated carbon which has an amorphous structure results in a high specific surface area and is able to increase its specific capacitance [28]. In addition, 70% of electrode samples consisting of activated carbon and carbon black also make the XRD diffraction pattern dominated by carbon peaks.

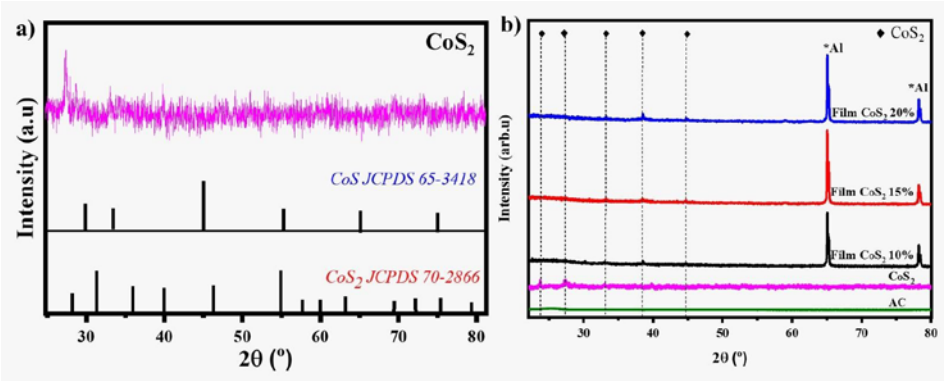

Fig. 2. XRD pattern of CoS_2 powder and film

XRD diffraction pattern of CoS_2 powder where the phase formed is amorphous. The results of the diffraction peak matching analysis indicate that the powder formed is CoS_2. Based on the analysis, the X-ray diffraction pattern shows that CoS_2 powder has peaks at diffraction angles 2θ = 8.56º, 23.73º and 27.34º in accordance with the JCPDS 70- 2866. The electrodes of each variation were also characterized by XRD to determine the composite material. The analysis showed the presence of $Ni(OH)_2$ peaks at diffraction angles 2θ = 19.19°, 33.27°, and 38.80°. While the CoS_2 peak is not visible due to its amorphous structure similar to the structure of activated carbon. Activated carbon which has an amorphous structure results in a high specific surface area and is able to increase its specific capacitance [28]. In addition, 70% of electrode samples consisting of activated carbon and carbon black also make the XRD diffraction pattern dominated by carbon peaks.

Activated carbon is a key material in the fabrication of supercapacitor-grade electrodes. The porous size of activated carbon is an important parameter in producing supercapacitors with good performance. Therefore, in this study, almost 70% of the main material is activated carbon. The presence of pores in the activated carbon was confirmed using SEM testing with various magnifications shown in Figure 3(a). At a magnification of 2,000 times, we can see chunks of activated carbon that have pores on their surface. The activated carbon pores in Figure 3(a) are clearly visible in the SEM results although the pore size is not too large. Porous carbon has a large surface area with a pore structure that facilitates ions in the energy storage process [29].

In addition to the powder material, SEM characterization was also performed on the electrode film. The SEM results of each electrode are presented in Figure 3(d-f) with SEM cross section illustration in Figure 3(g-i). From Figure 3(d-f), it can be seen that the electrodes are dominated by lump-shaped activated carbon as shown in Figure 3(a). At 2,500 times magnification, it can be seen that activated carbon has pores that are very favorable for the transfer of electrolyte ions into the electrode so as to improve the electrochemical performance of the electrode [30], [31]. The surface of the electrode is seen to agglomerate at some points caused by the interaction between activated carbon and PVDF (binder) [32]. SEM results also show CoS_2 and Ni(OH)2 nanoparticles that are not so visible because the percentage is less than activated carbon.

Electrode thickness also plays an important role in determining the electrochemical performance of supercapacitor devices because it can increase current density and energy density [33], [34]. However, electrodes that are too thick can also increase resistance and reduce the voltage applied to the electrode so that it will have an impact on reducing capacitance [35]. Therefore, it is necessary to determine the right thickness according to the material that makes up the electrode to get optimal performance [36]. The thickness of the electrode can be known from the cross-section results analyzed using ImageJ software. The

thickness of the 10% CoS_2 sample is 27.09 μm with an uneven electrode surface. In contrast, the thickness of the 15% CoS_2 sample is thinner at 11.15 μm, but also flatter than the other electrodes. 20% CoS_2 sample has a thickness of 45.69 μm. Based on these results, the electrode with the optimum thickness and flat surface is clearly owned by the 15% CoS_2 sample. In addition to electrode thickness, electrode porosity also affects the electrochemical performance of the supercapacitor. Porosity analysis was carried out using Origin Pro software.The porosity of the electrode film was analyzed using SEM results at 1000 times magnification. The porosity of the electrode film of each sample was 62.28%, 65.00% and 63.12%. This result shows that the highest porosity is owned by the 15% CoS_2 sample. A decrease in porosity is shown in the 20% CoS_2 sample which results in pore closure when exposed to the electrolyte so that changes in the electrochemical process occur.

Supercapacitor performance not only depends on the electrodes, but is also affected by

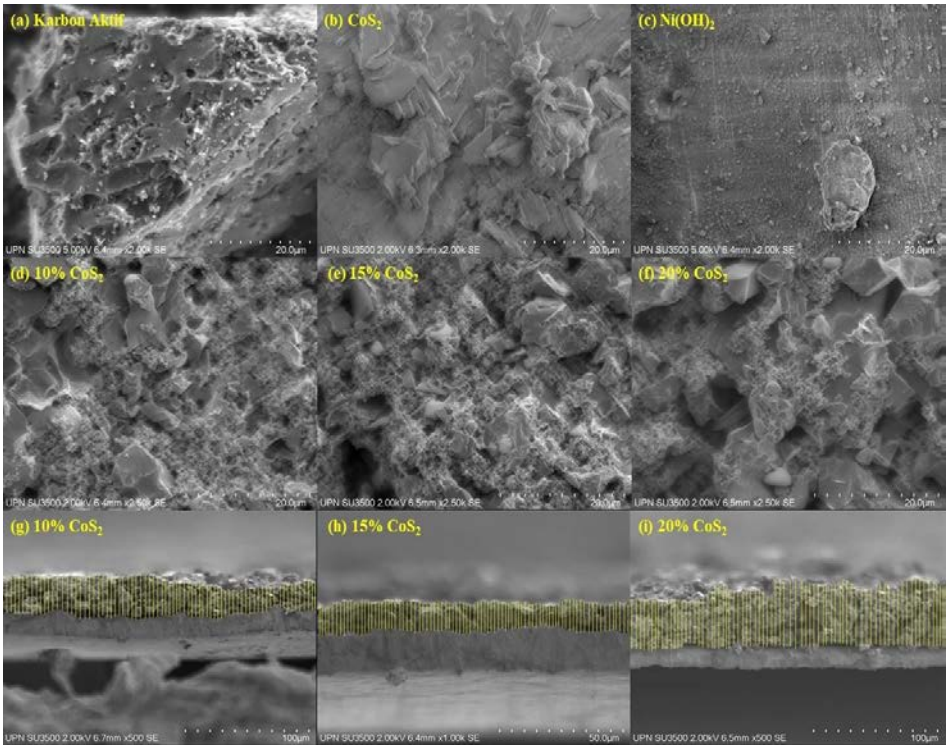

Fig. 3. Morphology of (a) activated carbon powder, (b) CoS_2 powder, (c) $Ni(OH)_2$ powder at 2000 times magnification and electrode (d) 10% CoS_2 film, (e) 15% CoS_2 film, (f) 20% film % CoS_2 at 2500 times magnification.

the electrolyte and separator used [37]. The separator used must be thin, electrochemically stable and have high ion conductivity [38]. Cloth fiber is widely used as a separator because it is thin and allows ions to diffuse easily [39]. The electrolyte that is often used is Et_4NBF_4 because it is an organic electrolyte. Et_4NBF_4 can be used on cheap current collectors such as aluminum with a voltage range of 2.5 - 2.8 Volts [40]. The electrochemical performance of supercapacitor electrodes can be known through cyclic voltammetry and charge discharge characterization using a 1 M Et_4NBF_4 solution as the electrolyte of a two-electrode system (coin cell) with a voltage of 1 Volt. Cyclic voltammetry is one of the most commonly used characterization techniques to determine the electrical and electrochemical properties of supercapacitor [41]. The extent of the cyclic voltammetry curve is used to determine the

specific capacitance of the supercapacitor [42]. The cyclic voltammetry curve is shown in Figure 4.

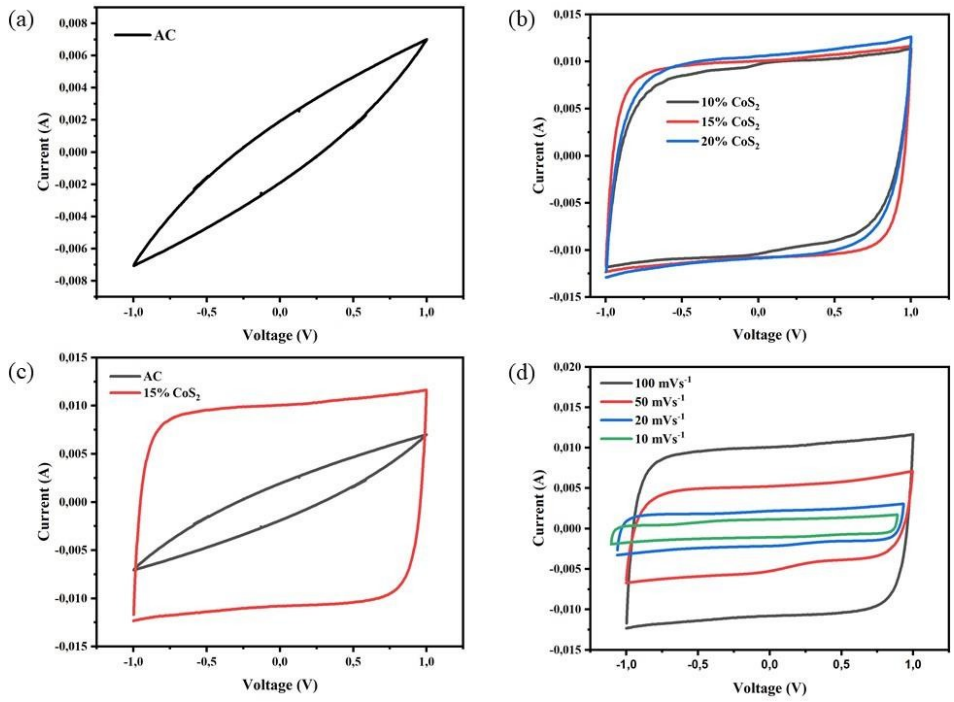

Fig. 4. Cyclic voltammetry curves (a) activated carbon at a scan rate of 100mVs^{-1}, (b) CoS_2 composite at a scan rate of 100mVs^{-1}, (c) AC and 15% CoS_2 at a scan rate of 100mVs^{-1} and (d) 15% CoS_2 at different scan rates.

The voltage used was 1 V with scan rates of 100, 50, 20 and 10 mVs^{-1}. The CV curve of the pure AC electrode in Figure 4(a) is formed at a scan rate of 100 mVs^{-1}. Figure 4(a) has a quasi rectangular shape which indicates an EDLC type electrode [43]. The CV curve in Figure 4(b) is the CoS_2 electrode at various mass variations measured at a scan rate of 100 mVs^{-1}. All three curves have an imperfect square shape indicating the performance of pseudocapacitors electrodes [44].

The difference from the curve in Figure 4(b) is the area of the curve formed. In the 10% CoS_2 sample, the resulting curve area is 0.0353, 15% CoS2 is 0.0394 and 20% CoS2 is 0.0389 which is the largest area in the 15% CoS_2 sample. When compared in Figure 4(c) between the activated carbon (AC) and 15% CoS_2 composite samples, the AC electrode has a smaller curve area, indicating that the transition metal composite plays a role in improving the performance of the supercapacitor. Table 1 shows the performance of the supercapacitor, where the 15% CoS_2 sample has the optimum capacitance of 21.93 Fg^{-1} which has the largest curve area.

Figure 4(d) shows the curve of 15% CoS_2 sample at various scan rates. The curve at a scan rate of 10 mVs^{-1} is formed without discontinuity indicating an increase in electron conduction within the electrode which favors rapid charge diffusion thus enhancing the good and stable capacitive performance of the electrode [45], [46]. Changes in the shape of the curve occur as the scan rate changes. Increasing the scan rate causes the chemical reaction to take place quickly so that the polarization of electrolyte ions occurs, electrolyte ions cannot enter the electrode porous [46], [47].

Table 1. Specific capacitance of supercapacitor at scan rate 100 mVs^{-1}.

Sample	Area	Specific Capacitance (F/g)
AC	0.0054	2.24
10% CoS2	0.0353	17.67
15% CoS2	0.0394	21.93
20% CoS2	0.0389	19.45

The electrochemical performance of supercapacitor $Ni(OH)_2$-CoS_2/Graphene Nanosheet//Carbon can be determined through charge discharge characterization. Figure 6 shows the supercapacitor charge discharge curve at a voltage of 0 - 1 Volt formed based on the relationship between voltage (V) and time (s). The charge discharge curve of the pure activated carbon supercapacitor coin cell (AC) in Figure 6(a) has an imperfect triangular shape at the end. The imperfect triangle shape is caused by a voltage drop that occurs suddenly or commonly called an IR drop of 0.1 V. In Figure 6(b) the best performance of the CoS_2 composite supercapacitor electrode is in the 15% CoS_2 sample which has the longest discharge time of about 225 seconds. When compared to the AC supercapacitor in Figure 6(c) the performance of the 15% CoS_2 composite supercapacitor is much better by a longer discharge time. Longer discharge times prove that hydroxide transition metal composites such as CoS_2 and $Ni(OH)_2$ and GNS improve supercapacitor performance [48]. The discharge time of the supercapacitor is directly proportional to the capacitance and inversely proportional to the potential difference. The capacitance, energy density and power density are shown in Table 2, respectively.

Table 2. Specific capacitance, energy density and power density at current density 0.1 Fg^{-1}

Sample	Spesific Capacitance (F/g)	Energy Density (Wh/kg)	Power Density (W/kg)
AC	44.62	0.98	45.84
10% CoS2	52.18	1.38	50.80
15% CoS2	58.25	1.57	70.49
20% CoS2	55.66	1.49	55.62

From Table 2, the largest specific capacitance is showed by the 15% CoS_2 sample with a specific capacitance of 58.25 Fg^{-1}. There was a decrease in capacitance in the 20% CoS_2 sample to 55.66 Fg^{-1} due to the resistance in the electrode thus inhibiting the reaction of the electrode and electrolyte [39]. The addition of too many transition metals also reduces the performance of supercapacitor, in general transition metals have low conductivity [49]. Figure 5(d) shows the 15% CoS_2 sample at different current densities, when the current density gets higher it makes the discharge time short. The increase in capacitance, energy density and power density of the supercapacitor shows that the most optimum electrochemical performance is achieved by the 15% CoS_2 sample.

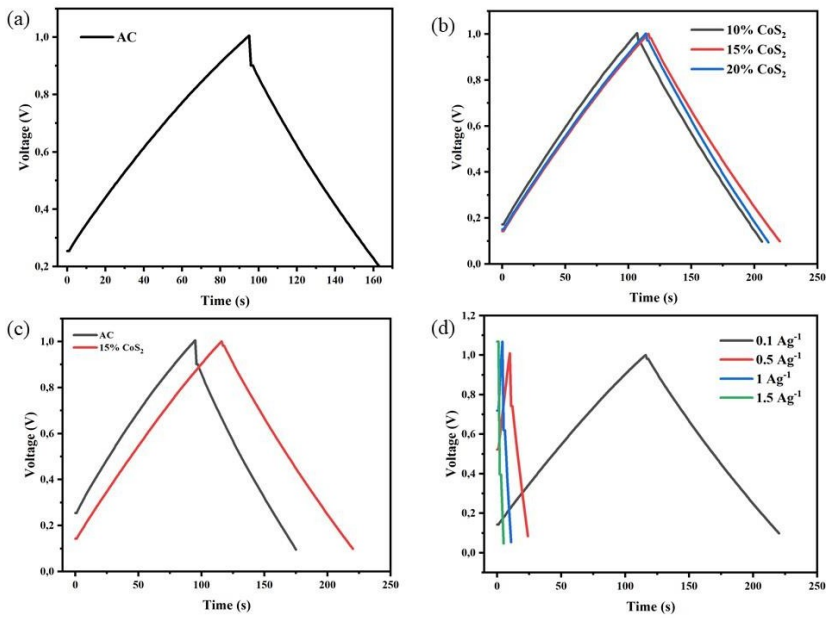

Fig. 5. Charge discharge curve (a) activated carbon at a current density of 0.1 Ag^{-1}, (b) CoS_2 composite at a current density of 0.1 Ag^{-1}, (c) AC and 15% CoS_2 at a current density of 0.1 Ag^{-1} and (d) 15% CoS_2 at different current densities.

4 Conclusion

Based on the research results and data analysis that has been done, it can be concluded that the composite electrode has $Ni(OH)_2$ peak, GNS and AC peaks do not appear because they are amorphous and CoS_2 peak does not appear on $Ni(OH)_2$-CoS_2/Graphene Nanosheet//Carbon electrode. The addition of CoS2 mass increases the porosity of the $Ni(OH)_2$-CoS_2/Graphene Nanosheet//Carbon electrode which reaches an optimum at 15% CoS_2 sample. The addition of CoS_2 mass increases the specific capacitance, energy density and power density of the $Ni(OH)_2$-CoS_2/Graphene Nanosheet//Carbon electrode and is optimum at 15% CoS_2 sample.

References

1. P. V. Shinde, N. M. Shinde, J. M. Yun, R. S. Mane, and K. H. Kim, “Facile Chemical Synthesis and Potential Supercapacitor Energy Storage Application of Hydrangea-type Bi $_2$ MoO $_6$,” ACS Omega, vol. 4, no. 6, pp. 11093–11102, Jun. 2019, doi: 10.1021/acsomega.9b00522.
2. A. A. Saleh, N. Ahmed, A. H. Biby, and N. K. Allam, “Supercapacitor electrode materials by Design: Plasma- induced defect engineering of bimetallic oxyphosphides for energy storage,” J. Colloid Interface Sci., vol. 603, pp. 478–490, Dec. 2021, doi: 10.1016/j.jcis.2021.06.125.
3. Q. Hu et al., “Core-shell MnO_2@CoS nanosheets with oxygen vacancies for high-performance supercapacitor,” J. Power Sources, vol. 446, p. 227335, Jan. 2020, doi: 10.1016/j.jpowsour.2019.227335.

4. J. J. William, I. M. Babu, and G. Muralidharan, “Spongy structured α-Ni(OH)$_2$: Facile and rapid synthesis for supercapacitor applications,” Mater. Lett., vol. 238, pp. 35–37, Mar. 2019, doi: 10.1016/j.matlet.2018.11.136.
5. L. Yu and G. Z. Chen, “Supercapatteries as High-Performance Electrochemical Energy Storage Devices,” Electrochem. Energy Rev., vol. 3, no. 2, pp. 271–285, Jun. 2020, doi: 10.1007/s41918-020-00063-6.
6. L. Yu and G. Z. Chen, “Redox electrode materials for supercapatteries,” J. Power Sources, vol. 326, pp. 604– 612, Sep. 2016, doi: 10.1016/j.jpowsour.2016.04.095.
7. N. M. Shinde, P. V. Shinde, J. M. Yun, R. S. Mane, and K. H. Kim, “Room-temperature chemical synthesis of 3-D dandelion-type nickel chloride ($NiCl_2$@NiF) supercapacitor nanostructured materials,” J. Colloid Interface Sci., vol. 578, pp. 547–554, Oct. 2020, doi: 10.1016/j.jcis.2020.04.021.
8. Y. Xiao, Y. Liu, F. Liu, P. Han, and G. Qin, “Wearable pseudocapacitor based on porous MnO2 composite,” J. Alloys Compd., vol. 813, p. 152089, Jan. 2020, doi: 10.1016/j.jallcom.2019.152089.
9. S. Cheng et al., “Energizing Fe_2O_3-based supercapacitors with tunable surface pseudocapacitance via physical spatial-confining strategy,” Chem. Eng. J., vol. 406, p. 126875, Feb. 2021, doi: 10.1016/j.cej.2020.126875.
10. M. Mandal et al., “A high-performance pseudocapacitive electrode based on CuO–MnO_2 composite in redox- mediated electrolyte,” J. Mater. Sci., vol. 56, no. 4, pp. 3325–3335, Feb. 2021, doi: 10.1007/s10853-020-05415- 7.
11. H. Jiang, Z. Wang, L. Dong, and M. Dong, “Co(OH)$_2$/MXene composites for tunable pseudo-capacitance energy storage,” Electrochimica Acta, vol. 353, p. 136607, Sep. 2020, doi: 10.1016/j.electacta.2020.136607.
12. J. Yus et al., “Semiconductor water-based inks: Miniaturized NiO pseudocapacitor electrodes by inkjet printing,” J. Eur. Ceram. Soc., vol. 39, no. 9, pp. 2908–2914, Aug. 2019, doi: 10.1016/j.jeurceramsoc.2019.03.020.
13. X. Li et al., “Layer-by-layer inkjet printing GO film anchored Ni(OH)$_2$ nanoflakes for high-performance supercapacitors,” Chem. Eng. J., vol. 375, p. 121988, Nov. 2019, doi: 10.1016/j.cej.2019.121988.
14. Y.-L. Liu et al., “Achieving Ultrahigh Capacity with Self-Assembled Ni(OH) $_2$ Nanosheet-Decorated Hierarchical Flower-like MnCo $_2$ O $_{4.5}$ Nanoneedles as Advanced Electrodes of Battery–Supercapacitor Hybrid Devices,” ACS Appl. Mater. Interfaces, vol. 11, no. 10, pp. 9984–9993, Mar. 2019, doi: 10.1021/acsami.8b21803.
15. G. Surender, F. S. Omar, S. Bashir, M. Pershaanaa, S. Ramesh, and K. Ramesh, “Growth of nanostructured cobalt sulfide-based nanocomposite as faradaic binder-free electrode for supercapacitor,” J. Energy Storage, vol. 39, p. 102599, Jul. 2021, doi: 10.1016/j.est.2021.102599.
16. M. W. Iqbal et al., “Facile hydrothermal synthesis of high-performance binary silver-cobalt-sulfide for supercapacitor devices,” J. Energy Storage, vol. 52, p. 104847, Aug. 2022, doi: 10.1016/j.est.2022.104847.
17. L. Jinlong, L. Tongxiang, Y. Meng, K. Suzuki, and H. Miura, “Comparing different microstructures of CoS formed on bare Ni foam and Ni foam coated graphene and their supercapacitors performance,” Colloids Surf. Physicochem. Eng. Asp., vol. 529, pp. 57–63, Sep. 2017, doi: 10.1016/j.colsurfa.2017.05.074.
18. H. Luo et al., “Engineering Ternary Copper-Cobalt Sulfide Nanosheets as High-performance Electrocatalysts toward Oxygen Evolution Reaction,” Catalysts, vol. 9, no. 5, p. 459, May 2019, doi: 10.3390/catal9050459.

19. M. Yu, X. Li, Y. Ma, R. Liu, J. Liu, and S. Li, “Nanohoneycomb-like manganese cobalt sulfide/three dimensional graphene-nickel foam hybid electrodes for high-rate capability supercapacitors,” Appl. Surf. Sci., vol. 396, pp. 1816–1824, Feb. 2017, doi: 10.1016/j.apsusc.2016.11.203.
20. H. Quan, B. Cheng, D. Chen, X. Su, Y. Xiao, and S. Lei, “One-pot synthesis of α-MnS/nitrogen-doped reduced graphene oxide hybrid for high-performance asymmetric supercapacitors,” Electrochimica Acta, vol. 210, pp. 557–566, Aug. 2016, doi: 10.1016/j.electacta.2016.05.031.
21. A. Mohammadi Zardkhoshoui, B. Ameri, and S. Saeed Hosseiny Davarani, “Fabrication of hollow $MnFe_2O_4$ nanocubes assembled by CoS_2 nanosheets for hybrid supercapacitors,” Chem. Eng. J., vol. 435, p. 135170, May 2022, doi: 10.1016/j.cej.2022.135170.
22. S. Y. Shajaripour Jaberi, A. Ghaffarinejad, Z. Khajehsaeidi, and A. Sadeghi, “The synthesis, properties, and potential applications of CoS_2 as a transition metal dichalcogenide (TMD),” Int. J. Hydrog. Energy, vol. 48, no. 42, pp. 15831–15878, May 2023, doi: 10.1016/j.ijhydene.2023.01.056.
23. Q. Wu, L. Liu, H. Guo, L. Li, and X. Tai, “Decorated by Cu nanoparticles CoS_2 nanoneedle array for effective water oxidation electrocatalysis,” J. Alloys Compd., vol. 821, p. 153219, Apr. 2020, doi: 10.1016/j.jallcom.2019.153219.
24. C. S et al., “A facile supercritical fluid synthesis of cobalt sulfide integrated with MXene and PANI/PEDOT nanocomposites as electrode material for supercapacitor applications,” FlatChem, vol. 37, p. 100456, Jan. 2023, doi: 10.1016/j.flatc.2022.100456.
25. W. Liu et al., “Cobalt disulfide/carbon nanofibers with mesoporous heterostructure and excellent hydrophilicity for high energy density asymmetric supercapacitor,” Nano Res., vol. 16, no. 7, pp. 10401–10411, Jul. 2023, doi: 10.1007/s12274-023-5533-1.
26. J. Xu et al., “Template strategy to synthesize porous Mn-Co-S nanospheres electrode for high-performance supercapacitors,” J. Energy Storage, vol. 44, p. 103267, Dec. 2021, doi: 10.1016/j.est.2021.103267.
27. F. Chen, Y. Ji, F. Ren, S. Tan, and Z. Wang, “Three-dimensional hierarchical core-shell $CuCo_2O_4$@$Co(OH)_2$ nanoflakes as high-performance electrode materials for flexible supercapacitors,” J. Colloid Interface Sci., vol. 586, pp. 797–806, Mar. 2021, doi: 10.1016/j.jcis.2020.11.004.
28. S. Iqbal, H. Khatoon, A. Hussain Pandit, and S. Ahmad, “Recent development of carbon based materials for energy storage devices,” Mater. Sci. Energy Technol., vol. 2, no. 3, pp. 417–428, Dec. 2019, doi: 10.1016/j.mset.2019.04.006.
29. B. Singu, E. S. Goda, and K. Yoon, “Carbon Nanotube–Manganese oxide nanorods hybrid composites for high- performance supercapacitor materials,” J. Ind. Eng. Chem., vol. 97, Feb. 2021, doi: 10.1016/j.jiec.2021.02.002.
30. B. K. Kim, S. Sy, A. Yu, and J. Zhang, “Electrochemical Supercapacitors for Energy Storage and Conversion,” in Handbook of Clean Energy Systems, J. Yan, Ed., Chichester, UK: John Wiley & Sons, Ltd, 2015, pp. 1–25. doi: 10.1002/9781118991978.hces112.
31. D. Bhattacharjya, D. Carriazo, J. Ajuria, and A. Villaverde, “Study of electrode processing and cell assembly for the optimized performance of supercapacitor in pouch cell configuration,” J. Power Sources, vol. 439, p. 227106, Nov. 2019, doi: 10.1016/j.jpowsour.2019.227106.

32. S.-H. Lee and J.-M. Kim, “Improved performances of hybrid supercapacitors using granule Li4Ti5O12/activated carbon composite anode,” Mater. Lett., vol. 228, pp. 220–223, Oct. 2018, doi: 10.1016/j.matlet.2018.06.006.
33. X. Yang et al., “Comparative evaluation of PPyNF/CoOx and PPyNT/CoOx nanocomposites as battery-type supercapacitor materials via a facile and low-cost microwave synthesis approach,” Electrochimica Acta, vol. 311, pp. 230–243, Jul. 2019, doi: 10.1016/j.electacta.2019.04.084.
34. A. M. Abdul Mageeth, S. Park, M. Jeong, W. Kim, and C. Yu, “Planar-type thermally chargeable supercapacitor without an effective heat sink and performance variations with layer thickness and operation conditions,” Appl. Energy, vol. 268, p. 114975, Jun. 2020, doi: 10.1016/j.apenergy.2020.114975.
35. S. Kumagai, K. Mukaiyachi, and D. Tashima, “Rate and cycle performances of supercapacitors with different electrode thickness using non-aqueous electrolyte,” J. Energy Storage, vol. 3, pp. 10–17, Oct. 2015, doi: 10.1016/j.est.2015.08.002.
36. F. Wang et al., “Electrode thickness design toward bulk energy storage devices with high areal/volumetric energy density,” Appl. Energy, vol. 289, p. 116734, May 2021, doi: 10.1016/j.apenergy.2021.116734.
37. M. Arvani et al., “Additive manufacturing of monolithic supercapacitors with biopolymer separator,” J. Appl. Electrochem., vol. 50, no. 6, pp. 689–697, Jun. 2020, doi: 10.1007/s10800-020-01423-2.
38. A. Pramitha and Y. Raviprakash, “Recent developments and viable approaches for high-performance supercapacitors using transition metal-based electrode materials,” J. Energy Storage, vol. 49, p. 104120, May 2022, doi: 10.1016/j.est.2022.104120.
39. M. Diantoro et al., “Hierarchical Activated Carbon–MnO_2 Composite for Wide Potential Window Asymmetric Supercapacitor Devices in Organic Electrolyte,” Micromachines, vol. 13, no. 11, Art. no. 11, Nov. 2022, doi: 10.3390/mi13111989.
40. C. Zhong, Y. Deng, W. Hu, J. Qiao, L. Zhang, and J. Zhang, “A review of electrolyte materials and compositions for electrochemical supercapacitors,” Chem. Soc. Rev., vol. 44, no. 21, pp. 7484–7539, Oct. 2015, doi: 10.1039/C5CS00303B.
41. J. Han, H. L. Chan, M. G. Wartenberg, H. H. Heinrich, and J. R. Scully, “Distinguishing interfacial double layer and oxide-based capacitance on gold and pre-oxidized Fe-Cr in 1-ethyl-3-methylimidazolium methanesulfonate room temperature ionic liquid aqueous mixture,” Electrochem. Commun., vol. 122, p. 106900, Jan. 2021, doi: 10.1016/j.elecom.2020.106900.